

Mehdi HABIBZADEH¹, Adam KRZYŻAK¹, Thomas FEVENS¹

APPLICATION OF PATTERN RECOGNITION TECHNIQUES FOR THE ANALYSIS OF THIN BLOOD SMEAR IMAGES

In this paper we discuss applications of pattern recognition and image processing to automatic processing and analysis of histopathological images. We focus on counting of Red and White blood cells using microscopic images of blood smear samples. We provide literature survey and point out new challenges. We present an improved cell counting algorithm.

1. MANUAL ANALYSIS OF BLOOD SMEAR IMAGES

Analysis of microscopic medical images is an important interdisciplinary problem involving both physicians and computer scientists. One of the important and active areas of research is the problem of counting blood cells (CBC) [12] which is used as screening test to check such disorders as infections, allergies, problems with clotting, and it helps diagnosing and managing a large number of diseases. In practice a panel of tests is carried out that examine different blood components such as counting white blood cells (WBC) [12-Ch.159, 1], white blood cells differential, counting red blood cells (RBC) [12-Ch.159], checking for signs of disease and the counting the number of infected cells. In normal human blood, there are 4,000,000-6,000,000, 4,000-11,000, 150,000-450,000 per microliter of RBC, WBC, and normal platelet counts, respectively, with platelets usually present in complexes rather than singularly [12]. But instead of the special case of spontaneous bleeding, platelet counts are rarely requested in a CBC, so in this work we will focus on RBC and WBC counts.

A manual diagnosis would search for abnormalities in the blood cells and particles while performing a CBC. Complications may arise from the large number of hematic pathologies [31] including the large number of WBC sub-types [22], which makes the analysis prone to human error. This process can be automated by computerized techniques which are more reliable and economical. Therefore there is always a need for the development of systems to provide assistance to hematologists and to relieve the physician of drudgery or repetitive work.

Our goal is to develop and validate an image processing and pattern recognition system to quantify and detect microscopic particles on thin blood smear slides to enhance automated system to characterize blood health status of patient. In essence we seek to determine a fast, accurate mechanism for segmentation and gather information about distribution of microscopic particles which may help to diagnose the degree of any abnormalities during clinical analysis. Automatic detection of pathologies from histopathological images is currently very active and important area of research.

2. AUTOMATIC PROCESSING OF BLOOD SMEAR IMAGES

During blood film examination, the individual types of blood smear particles (leukocytes and erythrocytes) are enumerated and then blood slides are usually made to investigate hematological problems [12]. The history of research into automated blood slide examination dates back to 1975, see Bentley & Lewis [3].

There is a vast amount of literature dedicated to differential blood counts. To aid in the segmentation of digital images, thresholding has been used as a pre-processing step [11]. But if the cells are relatively faint compared to the background, as is common with RBC in blood smear digital images,

¹ The Department of Computer Science and Software Engineering, Concordia University, Montréal, Québec, Canada H3G 1M8, email: {me_habi, krzyzak, fevens}@cse.concordia.ca.

this can lead to further problems which in turn require additional processing. Di Ruberto *et al.* [7] follow up the thresholding step by segmenting using classical morphological operators and the watershed algorithm [10] to demarcate cell boundaries.

Other common automatic approaches for boundary detection are active contours or snakes [17,25]. In addition to being dependent on the accurate placement of the initial contour, the boundaries of the cells detected may not follow the actual contours of the blood cells [26]. In related work [27] active contours were also used to track the boundaries of WBC but occluded cells were not accurately handled. Kumar *et al.* [18] introduced a new cell edge detector while trying to determine accurate nucleus edges. A two-step segmentation framework was proposed by Sinha and Ramakrishnan [35] using k-means clustering of the data mapped to HSV color space followed by using shape, color, and texture features in a neural network classifier. A watershed segmentation algorithm was used in [16] for WBC determination.

WBC classification in the recent work by Hamghalam *et al.* [14] utilizes Otsu's thresholding method to segment nuclei. The results are independent of the intensity differences in Giemsa-stained images of peripheral blood smear and active contours are used to extract precise boundary of cytoplasm.

As mentioned previously, the nature of automatic processing of microscopic images in medicine is a complicated task. This is because some of the basic tasks to be performed such as pre-processing, segmentation, classification, object recognition and inference require extensive understanding of the specific problem. This requires comprehensive knowledge in many disciplines such as medicine, computer science, image and signal processing.

3. METHODOLOGY AND ALGORITHMS

3.1. IMAGE GRAY SCALE CONVERSION

The normal blood images used in this research were saved in JPEG format of size 512×512 pixels. The first step in processing is to choose a proper gray scale channel. Some previous published work used the green channel of the RGB color encoding to analyze blood image data [8] or perform segmentation blood smear particles by choosing an appropriate threshold of this channel [21]. Also with the presence of white blood cells, granular cytoplasm pixels can be more easily separated from others in the image histogram of the G (green) channel (see Fig. 1 and [39]). We show that the best choice for converting the blood smear images to gray scale is to use the G channel rather than the other channels of the RGB encoding, or even the Y channel of YIQ encoding. The reason is that green channel is better at maintaining high frequency feature information and contrasts in gray scale intensity are more easily distinguished in the G channel.

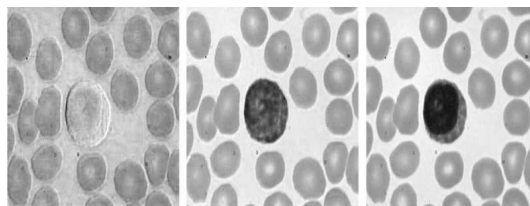


Fig. 1. (Left to right): Blue, Red, and Green channels (original, with no noise added; sample from Table 5).

Experiments on a set of 10 sample blood smear images show that the G channel has a wider range of gray-level values in the intensity histogram than the R and B channels and thus keeps more feature details (see Fig. 2). The G channel generally has the highest contrast between structures even in the presence of different backgrounds (e.g., different staining and/or different image capturing techniques) as compared to the R and B channels. Gray-level distributions of the three RGB channels for the sample image in Fig. 1 are shown in Fig. 2.

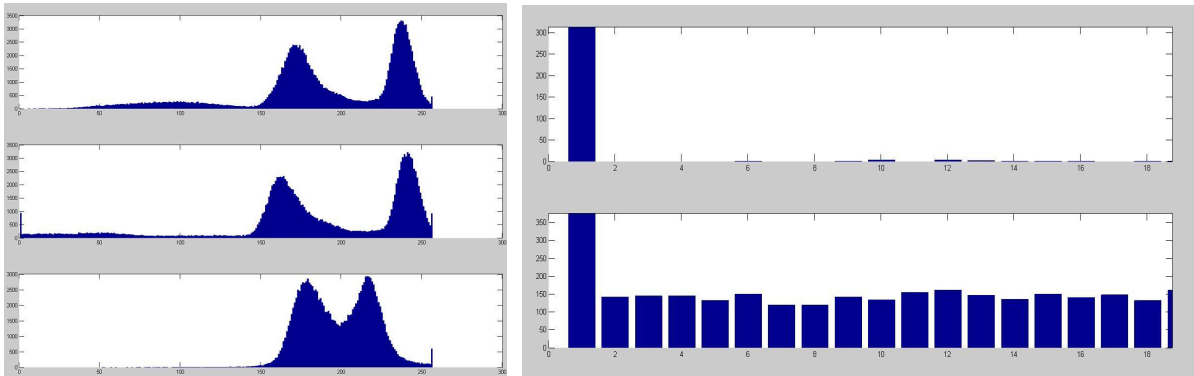


Fig. 2. Left: Gray scale distribution for image from Fig. 1, top to bottom: Red, Green, and Blue channels; Right: Zooming in on left side of distributions in Red (top) and Green (bottom) channels. The x-axis is the gray scale intensity from 0 to 255, and the y-axis is number of pixels at that gray scale intensity.

Table 1. Variances of individual color channels (RGB) over 10 blood images with different noise characteristics.

Color Channel	Image Characteristics	Variance
Red	normal images	$1.2395 \cdot 10^8$
Green	normal images	$1.4088 \cdot 10^8$
Blue	normal images	$0.94807 \cdot 10^8$
Red	additive medium noisy images	$2.19 \cdot 10^8$
Green	additive medium noisy images	$2.99 \cdot 10^8$
Blue	additive medium noisy images	$1.75 \cdot 10^8$
Red	additive high noisy images	$1.14 \cdot 10^8$
Green	additive high noisy images	$1.41 \cdot 10^8$
Blue	additive high noisy images	$0.82 \cdot 10^8$

The variance of a data set measures how far the values are spread out. We can validate better resolution of the G channel by considering variances of the three RGB channels (Table 1) over the set of 10 sample images (see Table 5) with different noise. The variance is consistently highest for the G channel.

We will consider YIQ color space in addition to RGB and HIS spaces. YIQ encoding is composed of two kinds of information, luminance Y and color information (I and Q). The main reason for introducing YIQ is specific sensitivity of human visual system which is more aware of changes in luminance than to changes in hue or saturation and thus a wider bandwidth should be dedicated to luminance than to color information. So, we also compare the Y channel with the G channel of the RGB color space. Since in YIQ encoding wide bandwidth is dedicated to the Y channel, the opacity and clearance of an object in Y channel is expected to be very comparable with G channel, compare Fig. 3 for a normal, no noise added sample from Table 5.

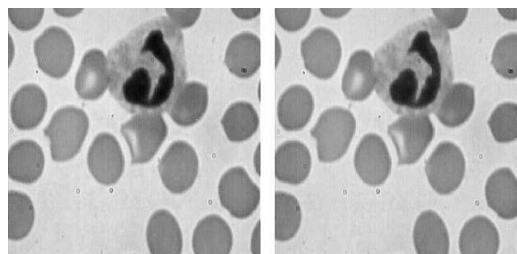


Fig. 3. Left to right: G channel (RGB encoding), Y Channel (YIQ encoding).

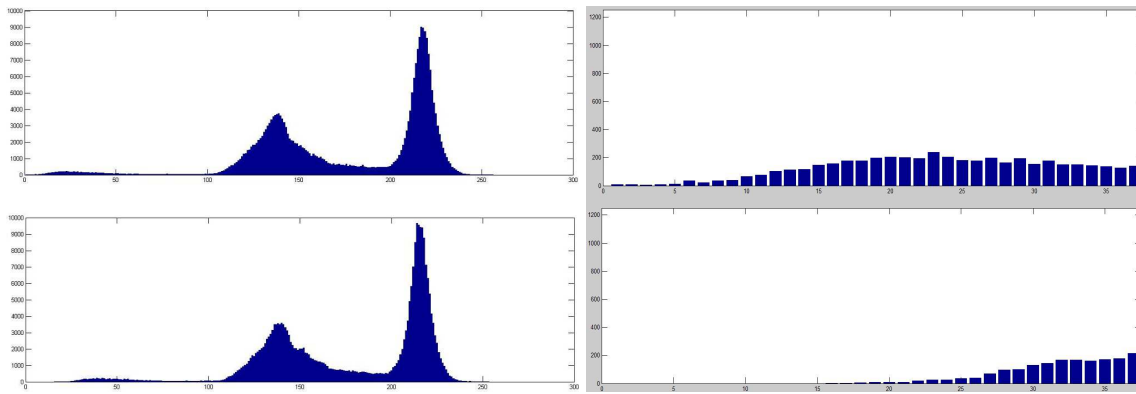


Fig. 4. Left: Gray scale distribution from the image in Fig. 1, top to bottom: G (RGB) and Y (YIQ) channels; Right: Zooming in on left size of distribution: G (RGB), Y (YIQ). The x-axis is the gray scale intensity from 0 to 255, and the y-axis is number of pixels at that gray scale intensity.

Table 2. Variance of G (RGB) and Y (YIQ) over 10 blood smear images with different noise characteristics.

Color channel	Image characteristics	Variance
G	normal images	$1.4088 \cdot 10^{08}$
Y	normal images	$1.2707 \cdot 10^{08}$
G	additive medium noisy images	$2.99 \cdot 10^{08}$
Y	additive medium noisy images	$1.47 \cdot 10^{08}$
G	additive high noisy images	$1.41 \cdot 10^{09}$
Y	additive high noisy images	$0.98 \cdot 10^{09}$

Experiments with the same 10 of blood smear images again show that the G channel has a wider range of gray-level values than Y channel outcome (Fig. 4). In addition, the variance is highest for the G channel (see Table 2). We conclude that the G channel is the most robust channel which maintains more details than other gray scale encodings, so this channel is selected for further processing as described next.

3.2. IMAGE DENOISING

Noise gives an image an undesirable visual appearance. However, the most dominant effect is that noise reduces the visibility of certain features within the image. Noise can be categorized into salt-pepper noise, Gaussian noise, speckle noise, etc. [30]. All medical and clinical images may contain some visual noise from a variety of sources but noise is much more prevalent in certain types of imaging procedures than in others. For example, noise is significant in Magnetic Resonance Imaging, Computerized Tomography, and Ultrasound Imaging, while Radiography produces images with the least amount of noise [36].

To design a reliable segmentation and cell counting system that may be used under different conditions such as a variety of blood smear staining techniques, types of chemical materials used, microscope types, illumination conditions, human error, etc., a denoising pre-processing step is required. One of the most practical and widely used denoising techniques is the wavelet shrinkage approach which thresholds the wavelet coefficients of an image. Wavelet coefficients having small absolute values are considered to encode mostly noise and very fine details of the signal. In contrast, the important information is encoded by the coefficients having large absolute values. Removing the small coefficients and then reconstructing the signal could produce signal with lesser amount of noise. The biggest challenge in the wavelet shrinkage approach is finding an appropriate threshold value [9].

The wavelet shrinkage approach can be summarized as follows:

1. Apply the wavelet transform to the signal,
2. Estimate a threshold value,
3. Remove (zero out) the coefficients that are smaller than the threshold,
4. Reconstruct the signal (apply the inverse wavelet transform)

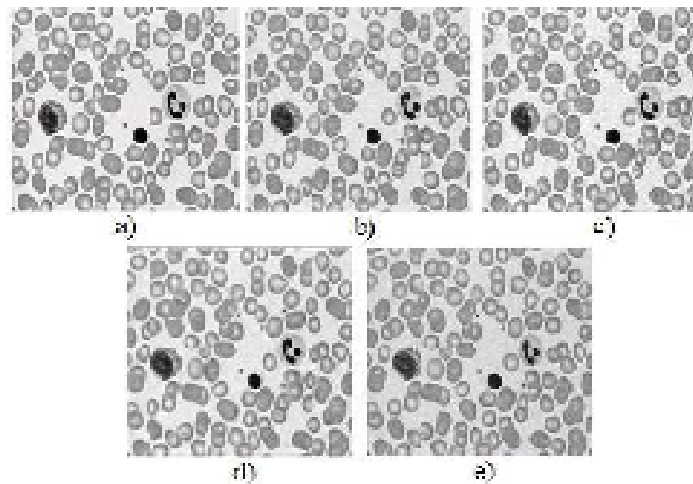


Fig. 5. Denoising techniques: a) original image; b) noisy image; c) median; d) soft thresholding; e) Bivariate.

In [33,34] Daubechies wavelet with soft thresholding and bivariate shrink filter has been used and the performance of the algorithms was compared according to the peak signal-to-noise ratio (PSNR). The optimal thresholding is obtained by tuning soft thresholding using experience and the type of images. In Fig. 5 we compare wavelet denoising with median denoising and bivariate denoising. The original images have been corrupted by moderate additive Gaussian noise with standard deviation 30, while Table 3 presents PSNR results for both moderate and high additive Gaussian noise with standard deviation 30 and 100, respectively.

Table 3. PSNR levels for various denoising techniques for images with moderate and high noise.

		Additive Noise Deviation	
		30	100
PSNR	noisy image	19.2149	10.4516
	image denoised by median filter	25.5666	16.5183
	image denoised by thresholding filter	23.546	18.3421
	image denoised by bivariate filter	27.6236	20.4822

From the experimental results it can be concluded that for moderate noise the Bivariate Shrink filter produces the best results. It produces the maximum PSNR for the output image compared to the other filters. However, the bivariate output is somehow blurred and some post-processing involving de-blurring and edge preserving may be needed. For images significantly corrupted by noise with low PSNR value (10.4516) the bivariate shrink filter is again the best. It produces the maximum acceptable PSNR for the output image compared to the other filters. It can also be observed that for high noise soft thresholding produces better results than the classical median filter.

3.3. EDGE PRESERVATION

Edge preservation is a technique to recover degraded and blurred boundaries in images while reducing the negative effect of noise in images. This step can serve as a preliminary step to binarization and object segmentation. Different edge preservation methods have been proposed including median filter symmetrical nearest neighbor (SNN) filter [15], convolution kernel filters [2], preserving color reduction method [24], bilateral techniques [37] and the Kuwahara filter [19,29]. The non-linear Kuwahara can be implemented by examining the four overlapping quadrant regions surrounding a pixel and then selecting the one with the smallest variance, and using the average as the central pixel value. Based on experimentation and the discussion presented in the original paper [19], due to the intrinsic characteristics (complex texture) of blood smear particles, we note that the Kuwahara has the sharpest edges which leads to better binarization in next step (see Fig. 6). However, the output maybe somewhat toothy.

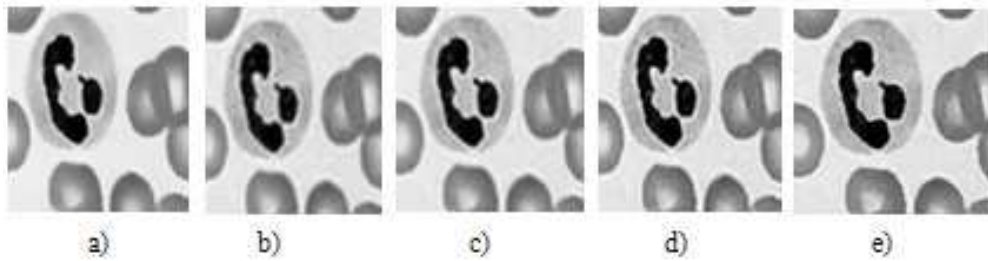


Fig. 6. Edge preservation: a) bilateral, b) convolution kernel, c) EDGEPS [36], d) SNN, and e) Kuwahara.

3.4. BINARIZATION WITH NIBLACK & OTSU

After pre-processing (denoising and edge enhancement) we applied several well-known binarization algorithms including Niblack [23], Bernsen [5], Sauvola [32] and Otsu [28] to improve foreground/background segmentation of blood smear microscopic images. Binarization is the last step before computing cell sizes and their enumeration. Binarization can be applied with either global or local thresholding.

For the global approach, a constant intensity threshold value T (between 0 and 255) is chosen. If the intensity value of any pixel (in the grey scale) of an input image is greater than T , then pixel is set to white otherwise it is set to black. However, in practice we have a variety of intensities of grey in the foreground and background. In blood smear slides, because of different kinds of image acquisition, illumination, staining, and since there are frequently overlapping and very closely positioned particles, finding a global value T to separate the slide into two ideal regions of blood particles and background is not always simple and perhaps not even possible (closely positioned pairs of particles will be merged into single particles, regardless of any fine tuning of the value of T).

To our knowledge, there are no comparative evaluations of the efficiency of binarization algorithms at binarizing medical blood smear images. Here we aim at determining the binarization algorithm best suited for microscopic blood smear images. Some papers on blood segmentation such as [4] used Otsu approach (one of the most popular threshold selection methods [39]) using global thresholding. In Niblack [23], the local thresholding is based on $T(x, y) = m(x, y) + k * s(x, y)$, where $m(x, y)$ and $s(x, y)$ are the average and the standard deviation of a local area for which the size of the window must be large enough to suppress noise in the image while at the same time it has to be small enough to maintain local details. The value of k decides how much of the total print object boundary is taken as a part of the given object. Coefficient k helps to separate and adjust the percentage of pixels that belong to foreground (especially in the boundaries). In the experiment involving Niblack algorithm 15×15 neighborhood and $k=0.1$ are selected.

We propose a more efficient and more accurate binarization method by combining the Otsu (global thresholding) and Niblack (local thresholding) approaches. In particular, we aim at more accuracy in terms of minimizing the number of close pairs of particles that are merged into single particles during binarization process.

To determine the best binarization algorithm, we determine the statistical significance between the algorithms by using the normalized cross-correlation (NCC) approach $\gamma(u, v)$ (see Eq. 1) which is often used in template matching and pattern recognition problems for determining the degree of similarity between two images [6]. In practice, the performance and reliability of binarization algorithm for a gray scale image is defined as the value of the NCC to quantify the similarity between two images A and B (as a template matching using green channel output of each image). If A exactly matches B then γ (the array of correlation coefficients) is equal to 1 while in cases of exact dissimilarity result in $\gamma=0$. In general, the coefficients in γ typically vary between -1 and +1.

$$\gamma(u, v) = \frac{\sum_{x,y} [A(x, y) - \bar{A}_{u,v}] [B(x-u, y-u) - \bar{B}]}{\left\{ \sum_{x,y} [A(x, y) - \bar{A}_{u,v}]^2 \sum_{x,y} [B(x-u, y-u) - \bar{B}]^2 \right\}^{1/2}} \quad (1)$$

The resulting coefficients in the matrix of NCC cannot all be the same and the measurement of performance and efficiency are subjected to a comparison using the average (expressed as the mean, median, and mode), standard deviation and range to show how much variation or dispersion there is between existing values.

Table 4. Summary of NCC data for each binarization algorithm performance over three different cases: (top to bottom) total over 10 regular blood smear images (N0–N9); total over 10 normal and regular separated WBCs; total over few disjoint close RBCs in 10 regular images (N0–N9).

10 Normal and Regular Images							
Algorithm	Mean	Median	Mode	StdDev	Range	Min	Max
Otsu	-0.0094	-0.0111	0	0.9410*10 ⁵	1.0803	-0.1866	0.8937
Bernsen	-0.0096	-0.0101	0	1.16*10 ⁵	0.7935	-0.2882	0.5055
Sauvola	-0.0111	-0.0150	0	1.53*10 ⁵	0.6727	-0.2754	0.3973
Niblack	-0.0111	-0.0143	0	1.468*10 ⁵	0.7328	-0.2654	0.4674
Normal and Regular WBCs images							
Algorithm	Mean	Median	Mode	StdDev	Range	Min	Max
Otsu	0.0259	0.0459	0	3.0834*10 ⁵	1.2122	-0.3870	0.8252
Bernsen	0.0262	0.0437	0	0.3987*10 ⁵	1.1234	-0.4192	0.7042
Sauvola	0.0304	0.0390	0	0.5008*10 ⁵	1.0516	-0.4021	0.6495
Niblack	0.0310	0.0383	-0.4320	0.5222*10 ⁵	1.0942	-0.4320	0.6622
Normal and Regular RBCs images							
Algorithm	Mean	Median	Mode	StdDev	Range	Min	Max
Otsu	0.0083	-0.0094	0	886.7119	1.1373	-0.2159	0.9214
Bernsen	0.0111	-0.0029	-0.0283	206.1605	0.9564	-0.2439	0.7125
Sauvola	0.0150	0.0114	0	216.3476	0.9460	-0.2852	0.6608
Niblack	0.0158	0.0153	0	227.5969	0.9023	-0.3206	0.5816

In our experimentation to study the effect of noise on binarization results, we degrade the objects (foreground) in samples by adding Gaussian and speckle noise to simulate the worst cases that may appear in image capturing. Also to simulate dirty slides or camera lens a 2, 3 pixel Gaussian blur is applied. The NCC results are presented in Tables 4a (on general blood smear images), 4b (impact of binarization on WBC) and 4c (considering the effect of binarization on RBC). In terms of NCC values the highest means are generated by Otsu as a global thresholding and the dispersion and variation are low which prove the acceptable degree of similarity between image and its template. However, in WBC segmentation and discrimination between WBCs and RBCs this approach may not work and also may join disjoint close objects as it uses global thresholding over all slides and of course cannot maintain all local details by again using global thresholding over all slides (see Fig. 7c, d). WBCs nucleus and cytoplasm intensity differs from intensity of dominant of RBCs and as the number of RBCs is about 100 times larger than WBCs in normal blood smear then global thresholding is influenced by RBCs rather than WBCs. Therefore, WBC boundary and its components are degraded and damaged by Otsu global thresholding in spite of having higher template matching. We investigate this problem by running each of four algorithms (see Fig. 7) and binarizing the samples containing single WBCs and also another subset of samples including a few RBCs (see Fig. 7 with two or three maximum disjoint RBCs with small gaps between objects). The NCC values are collected from a single run over sub-images (WBCs & few RBCs) yielding higher NCC values related to Niblack in these cases. With Niblack algorithm, in spite of higher NCC in these small windows (masks), local thresholding produces spurious objects and noisy spots despite minor intensity value differences in the background region, therefore the resulting binarized image always has noise in the background area, even if the proper local threshold k value is chosen. Thus we use two criteria to reconcile higher NCC in small windows (Niblack) (see Tables 4b and 4c)

including WBCs and few neighboring RBCs (better segmentation in foreground) and higher NCC in global thresholding by Otsu (see Table 4a) to avoid having spurious spots in background.

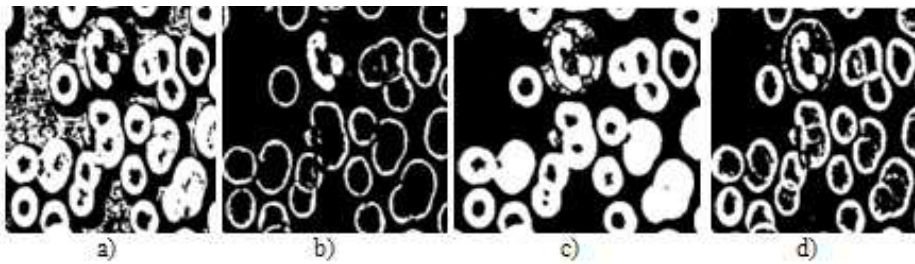


Fig. 7. Binarization results using the algorithm of: a) Bernsen; b) Sauvola; c) Otsu; and d) Niblack.

Computer experiments with different samples and initial conditions (see Fig. 7) show that Niblack approach is the most reliable method to maintain disjoint components which is crucial in avoiding over or under segmentation. In the previous work [4] Otsu thresholding was used for binarization; however, this method tends to result in overlapping objects that are too close to one another which in turn leads to false results after segmentation. In our modified version pixels are labeled as background pixels if they are labeled as either background pixels in Niblack or in Otsu and the remaining pixels are kept as foreground pixels (objects). Using this merging process, we mitigate the problem of extra small spurious regions produced by the Niblack algorithm.

3.5. SIZE ESTIMATION

Binarization and some post-processing to enhance the quality of binary image is followed by feature extraction which helps to differentiate different particles in the image. A normal blood sample typically contains two major particles: RBC with a normal size probability distribution function (PDF) with average size around 6.0-8.5 μm and WBC with average size around 7-18 μm including nucleus and cytoplasm and being about 1-3 times bigger than the normal and mature RBCs. We use size characteristics as an effective factor to distinguish between the two main types of cells. Granulometry [38] can determine the size distribution of image objects without explicitly segmenting each object first. According to normal blood PDF and RBC to WBC ratio, the maximum regional peak in pattern spectrum diagram correlates to the number of RBCs with an acceptable RBC radius size.

Granulometry uses structure elements which are morphologically dilated to the maximum size and applied to the image. The shape of structure element depends on the type of objects under processing. During the process granulometric density function is determined. The granulometric algorithm starts by applying an opening morphology along with defined structure element (SE). In normal blood smear images, all available particles are approximately circular. Hence, we select (disk) shape as default (SE) for granulometric algorithm. In an ideal output, we expect only one peak for a single complete circle, but the incomplete circular object shown in Fig. 8 produces local maxima. We call this undesirable effect an edge fracture. We just observe that after applying the edge detection and skeletonization algorithms to real cell images which are typically not complete curves the observed circular pieces are regarded as a new objects surrounded between two ideal complete circles. Consequently we can expect in granulometric output at least two local regional peaks. By this simple work, we find that blood smear particles are not complete circular object and there are always discrete components on curve tracer, which is another reason for undesirable local maxima.

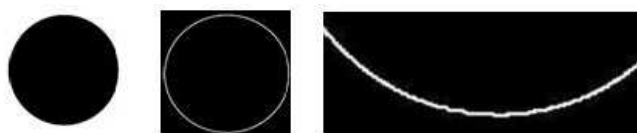


Fig. 8. Granulometry over simple circle.

Overall, applying granulometry to RBCs images in normal blood smear can be very reliable in determination and estimating their size. But for abnormal samples with different shapes or with extra overlapping between the particles granulometric approach may fail.

3.6. SEGMENTATION AND COUNTING ALGORITHM

Two sub-images containing individual WBCs indicators and RBCs are separated in order to count peripheral cells. This is done in two main procedures explained in detail in [13]. There are different methods which are directly or indirectly used to separate and segment objects in disjoint images such as active contours and watershed. Typically watershed is incorporated into the immersion and toboggan methods [20]. The accuracy and efficiency of watershed segmentation over images is directly related to the previous steps. In practice, a watershed algorithm works best for smooth convex objects that don't overlap too much. It cannot be an efficient approach in all microscopic images with extra overlapping which can happen for some diseases.

A set of 10 different blood smear test images with a vast variety of image characteristics from a normal thin blood film till very degraded blurry image (see the sample table) were used to show that the proposed framework is accurate and also is robust for degraded images which are blurry and (or) noisy. In Table 5 ten blood smear slides (numbered N0 through N9) are denoised by bivariate wavelet approach within our framework. The computed blood cell count results are compared with manual counts of the number of RBCs and WBCs (the differences between the computed counts and the manual counts are numbers in parenthesis). In the last four rows of Table 5, also the proficiency of the denoising approach was tested by using different additive noise over images in two different noise variance values at high (variance=150, mean=0) and medium (variance=30, mean=0) levels.

In Table 6, we give confusion matrices (with normalized rows) of the framework when applied to normal, moderately noisy and highly noisy blood smear images. In particular, for normal images, 90% of known RBCs were classified as such, with this classification rate decreasing to 78% for moderately noisy images, and then to 58% for highly noisy images. So, based on the confusion matrices with three classes: RBC, WBC and others composed of platelets and other possible existing parasites (in abnormal cases) the proposed consecutive steps are reliable and accurate even in presence of moderate and high level noise yielding acceptable accuracy.

Table 5. Experimental results of ten different blood smear images (numbered N0–N9). Counts for RBCs and WBCs are given from manual counts, as well as determined by our framework using Bivariate denoising. Values given in parentheses are the differences between counts computed and those obtained by a manual count (negative values indicate an under count; positive values indicate an over count).

Image #	Image Characteristics	Manual Count		Our frame work	
		RBC	WBC	RBC	WBC
N0	normal sample	104	1	98(-6)	1(0)
N1	without WBCs	75	0	66(-9)	0(0)
N2	blurred and overlapped	125	2	110(-15)	2(0)
N3	normal sample	105	3	99(-6)	3(0)
N4	Blurred	325	1	314(-11)	1(0)
N5	Blurred	66	2	62(-4)	2(0)
N6	numerous overlapping	90	2	76(-14)	2(0)
N7	WBCs touch RBCs	18	1	16(-2)	1(0)
N8	WBCs touch RBCs	69	2	65(-4)	2(0)
N9	blurred,numerous overlaps,WBCs touch RBCs	101	1	83(-18)	2(1)
N6	additive medium noise	90	2	77(-13)	3(1)
N9	additive medium noise	120	1	78(-42)	2(1)
N6	additive high noise	90	2	70(-20)	1(-1)
N9	additive high noise	120	1	81(-39)	5(4)

Table 6. Confusion matrices for proposed framework (left to right) total over 10 regular (N0–N9); 6 with moderate noise (N1, N2, N5, N6, N8, and N9); same 6 images with high noise.

Known	Assigned		
	RBC	WBC	Other
RBC	0.9	0	0.1
WBC	0.08	0.87	0.05
Other	0.31	0	0.69

Known	Assigned		
	RBC	WBC	Other
RBC	0.78	0.05	0.17
WBC	0	1	0
Other	0.16	0	0.84

Known	Assigned		
	RBC	WBC	Other
RBC	0.58	0.02	0.21
WBC	0.5	0.5	0
Other	0.23	0	0.77

4. FUTURE WORK AND CHALLENGES

Automatic CBC (complete blood count) is a challenging problem. It involves classification of WBC into five main categories such as basophils, eosinophils, lymphocytes, monocytes and neutrophils, and detection and categorization of pathologies such as anemias, leukaemias, lymphomas, cholera, malaria and many others. As different WBC and pathologies may be differentiated by shape, texture, color and other visual cues advanced image processing and machine learning techniques need to be utilized to build reliable classification systems. An important problem to address is the separation of different WBCs classes, as well as the identification of deformed RBC and WBC shapes with diseases such as malaria, leukemia, anemia, etc. This will be accomplished using cutting edge image segmentation techniques in combination with advanced machine learning techniques for classification, with the goal of improving the accuracy of CBC reports.

5. CONCLUSIONS

In this paper we discussed automatic processing and recognition of histopathological images of red and white blood cells. An efficient algorithm for fully automated detection and segmentation of blood cells microscopic imagery has been presented. The algorithm is accurate and offers remarkable segmentation accuracy. There are many challenging problems in automatic processing of histopathologies. The main problems include large variation of blood cells, occlusions, low quality of images and difficulties in getting real data. These problems will be addressed in the future work.

BIBLIOGRAPHY

- [1] AL-MUHAIRY J., AL-ASSAF Y., Automatic white blood cell segmentation based on image processing, In 16th IFAC World Congress, 2005.
- [2] BABIC Z., MANDIC D., An efficient noise removal and edge preserving convolution filter, In 6th International Conference on Telecommunications in Modern Satellite, Cable and Broadcasting Service, Vol. 2, 2003, pp. 538-541.
- [3] BENTLEY S., LEWIS, S., The use of an image analyzing computer for the quantification of red cell morphological characteristics, British Journal of Hematology, Vol. 29, 1975, pp. 81–88.
- [4] BERGEN T., STECKHAN D., WITTENBERG T., ZERFASS T., Segmentation of leukocytes and erythrocytes in blood smear images, In 30th Annual International Conference of the IEEE on Engineering in Medicine and Biology Society, 2008, pp. 3075–3078.
- [5] BERNSEN J., Dynamic thresholding of grey-level images, In International Conference on Pattern Recognition, 1986, pp. 1251–1255.
- [6] BOBIER B., WIRTH M., Evaluation of Binarization Algorithms, Tech. rep., Department of Computing and Information Science, University of Guelph, Guelph, ON, 2008.
- [7] DI RUBERTO C., DEMPSTER A., KHAN S., JARRA B., Segmentation of blood images using morphological operators, In 15th International Conference on Pattern Recognition, IEEE, Barcelona, Spain, 2000, pp. 397–400.
- [8] DI RUBERTO C., DEMPSTER A., KHAN S., JARRA, B., Analysis of infected blood cell images using morphological operators, Image and Vision Computing, Vol. 20, No. 2, 2002, pp. 133–146.
- [9] FODOR I., KAMATH C., On denoising images using wavelet-based statistical techniques, Tech. rep., Lawrence Livermore National Laboratory, 2001, UCRL JC-142357.

- [10] GAUCH J., Image segmentation and analysis via multiscale gradient watershed hierarchies, *IEEE Transactions on Image Processing*, Vol. 8, No. 1, 1999, pp. 69–79.
- [11] GONZALEZ R., WOODS R., *Digital Image Processing*, 3rd Economy Ed., Prentice–Hall, 2008.
- [12] GOOLDMAN L., SCHAFER A., The peripheral blood smear, In *Cecil Medicine*, Eds., 24, Saunders Elsevier, Philadelphia, PA, 2011, ch. 160.
- [13] HABIBZADEH M., KRZYŻAK A., FEVENS T., SADR A., Counting of RBCs and WBCs in noisy normal blood smear microscopic images, In *SPIE Medical Imaging*, Vol. 7963, 2011, pp. 79633I.
- [14] HAMGHALAM M., MOTAMENI M., KELISHOMI A.E., Leukocyte segmentation in giemsa-stained image of peripheral blood smears based on active contour, In *International Conference on Signal Processing Systems*, IEEE Computer Society, Los Alamitos, CA, USA, 2009, pp. 103–106.
- [15] HONG V., PALUS H., PAULUS D., Edge preserving filters on color images, *Lecture Notes in Computer Science* Vol. 3039, 2004, pp. 34–40.
- [16] JIANG K., LIAO Q.M., DAI, S.Y., A novel white blood cell segmentation scheme using scale-space filtering and watershed clustering, In *Int. Conf. on Machine Learning and Cybernetics*, Vol. 5, 2003, pp. 2820–2825.
- [17] KASS M., WITKIN A., TERZOPOULOS D., Snakes: Active contour models, *International Journal of Computer Vision* 4, 1988, pp. 321–331.
- [18] KUMAR B., JOSEPH D., SREENIVAS T., Teager energy based blood cell segmentation, In *International Conference on Digital Signal Processing*, Vol. 2, 2002, pp. 619–622.
- [19] KUWAHARA M., HACHIMURA K., EIHO S., KINOSHITA M., Processing of ri-angiocardigraphic images, In *Digital Processing of Biomedical Images*, PRESTON K., ONOE M., Eds., Plenum Press, New York, 1976, pp. 187–203.
- [20] LIN Y.C., TSAI Y.P., HUNG Y.P., SHIH Z.C., Comparison between immersion-based and toboggan-based watershed image segmentation, *IEEE Transactions on Image Processing*, Vol. 15, No. 3, 2006, pp. 632–640.
- [21] MAKKAPATI V., Improved wavelet-based microscope autofocusing for blood smears by using segmentation, In *IEEE Inter. Conf. on Automation Science & Engineering*, 2009, pp. 208–211.
- [22] MESCHER A., *Junqueira’s Basic Histology*, 12th Edition: Text and Atlas., McGraw-Hill Medical, 2009.
- [23] NIBLACK W., *An Introduction to Digital Image Processing*, Prentice-Hall, Inc., USA, 1990.
- [24] NIKOLAOU N., PAPAMARKOS N., Color reduction for complex document images, *International Journal of Imaging Systems and Technology*, Vol. 19, No. 1, 2009, pp. 14–26.
- [25] ONGUN G., HALICI U., LEBLEBICIOGLU K., ATALAY V., BEKSAC S., BEKSAC M., An automated differential blood count system, In *IEEE Int. Conf. on Engineering in Medicine and Biology Society*, Vol. 3, 2001, pp. 2583–2586.
- [26] ONGUN G., HALICI U., LEBLEBICIOGLU K., ATALAY V., BEKSAC S., BEKSAC M., Automated contour detection in blood cell images by an efficient snake algorithm, *Nonlinear Analysis-Theory Methods & Applications*, Vol. 47, No. 9, 2001, pp. 5839–5847.
- [27] ONGUN G., HALICI U., LEBLEBICIOGLU K., ATALAY V., BEKSAC M., BEKSAC S., Feature extraction and classification of blood cells for an automated differential blood count system, In *International Joint Conference on Neural Networks*, Vol. 4, 2001, pp. 2461–2466.
- [28] OTSU N., A threshold selection method from gray-level histograms, *IEEE Transactions on System, Man and Cybernetics*, Vol. 9, No. 1, 1979, pp. 62–66.
- [29] PAPARI G., PETKOV N., CAMPISI P., Artistic edge and corner enhancing smoothing, *IEEE Transactions on Image Processing*, Vol. 16, No. 10, 2007, pp. 2449–2462.
- [30] PATIDAR P., GUPTA M., SRIVASATAVA S., NAGAWAT A., Image de-noising by various filters for different noise, *International Journal of Computer Applications*, Vol. 9, 2010, pp. 45–50.
- [31] PIURI V., SCOTTI F., Morphological classification of blood leucocytes by microscope images, In *IEEE International Conference on Computational Intelligence Far Measurement Systems and Applications*, Boston, MA, 2004.
- [32] SAULOVA J., PIETIKAINEN M., Adaptive document image binarization, *Pattern Recognition*, Vol. 33, No. 2, 2000, pp. 225–236.
- [33] SENDUR L., SELESNICK I., A bivariate shrinkage function for wavelet-based denoising, In *IEEE International Conference on Acoustics, Speech, and Signal Processing*, Vol. 2, 2002, pp. 1261–1264.
- [34] SENDUR L., SELESNICK I., Bivariate shrinkage functions for wavelet-based denoising exploiting interscale dependency, *IEEE Transactions on Signal Processing*, Vol. 50, No. 11, 2002, pp. 2744–2756.
- [35] SINHA N., RAMAKRISHNAN A., Automation of differential blood count, In *Conf. on Convergent Technologies for Asia-Pacific Region*, Vol. 2, 2003, pp. 547–551.
- [36] SPARAWLS P., *Physical Principles of Medical Imaging* Second Edition, Medical Physics Pub, 1995.
- [37] TOMASI, C., MANDUCHI R. Bilateral filtering for gray and color images, In *Sixth International Conference on Computer Vision*, 1998, pp. 839–846.

- [38] VINCENT L., Fast opening functions and morphological granulometries, Image Algebra and Morphological Image Processing V, SPIE Proceedings, Vol. 2300, 1994, pp. 253–267.
- [39] WANG M., CHU R., A novel white blood cell detection method based on boundary support vectors, In IEEE International Conference on Systems, Man and Cybernetics, SMC'09, IEEE Press, 2009, pp. 2595–2598.